Surface & Coatings Technology 203 (2008) 357–363

Contents lists available at ScienceDirect

Surface & Coatings Technology

journal homepage: www.elsevier.com/locate/surfcoat

Morphology of metallic nanoparticles as a function of deposition time in electroless deposition of metal on multi-walled carbon nanotubes

Jeong Hoon Byeon [a], Jungho Hwang [b,c,*]

[a] Digital Printing Division, Samsung Electronics Co., Ltd., Suwon 443-742, Republic of Korea
[b] School of Mechanical Engineering, Yonsei University, Seoul 120-749, Republic of Korea
[c] Yonsei Center for Clean Technology, Yonsei University, Seoul 120-749, Republic of Korea

ARTICLE INFO

Article history:
Received 8 June 2008
Accepted in revised form 10 September 2008
Available online 19 September 2008

PACS codes:
81.05.Ni Dispersion-, fiber-, and platelet- reinforced metal-based composites
81.05.Rm Porous materials, granular materials
81.15.-z Methods of deposition of films and coatings, film growth, and epitaxy
81.16.Hc Catalytic methods
82.45.Aa Electrochemical synthesis
82.45.Jn Surface structure, reactivity and catalysis
82.45.Mp Thin layers, films, monolayers, membranes

Keywords:
Nanoparticles morphology
Multi-walled carbon nanotubes
Electroless deposition

ABSTRACT

Morphology of silver (or copper) nanoparticles as a function of deposition time was examined in electroless deposition of metal on multi-walled carbon nanotubes (MWCNTs). Silver (or copper) deposited MWCNTs were prepared using successively, surface oxidation, tin-palladium activation, hydrochloric acid-acceleration, and ELD of silver (or copper). The results show that nanoparticles of face-centered cubic silver (or copper) were deposited initially on the interior surface of a MWCNT (~50 nm in inner diameter) but later on its exterior surface. The percentage silver (or copper) in the coated MWCNTs increased from 7.0 (6.7) to 28.2 (25.5) wt.% by weight for a deposition time ranging from 3 to 10 min. The average diameter of silver (copper) nanoparticles increased from 1.3 (1.1) to 2.6 (2.3) nm, while the surface area and pore volume decreased from 261 to 144 (81) m^2/g and from 1.02 to 0.38 (0.27) cm^3/g, respectively. However, there was no silver deposition on the interior surface of a thin-MWCNT (~5 nm in inner diameter) observed because the capillarity decreases with decreasing tube diameter.

1. Introduction

Multi-walled carbon nanotube (MWCNT) is an ideal raw material for various applications owing to its outstanding properties [1]. Its high length:diameter ratio, strength, flexibility [2], unique conductivity [3], and other properties have led many to envision its application in areas like reinforced polymer composites [4] and nanosized electronic devices. Metal particle-supported MWCNTs are expected to be potential future materials [5–7] for hydrogenation catalysis or as materials in fuel cells, Li-ion batteries, supercapacitors, magnetic recording, reinforcements or for microwave absorption [5,8,9]. Various metal nanoparticles have been reported recently, such as Cu [9,10], Ni [11], Pt [12,13], and Au [3,13,14]. Previous approaches to functionalizing of MWCNTs with metal nanoparticles [15–19] include physical evaporation, attachment after the oxidation of nanotubes, solid state reaction with metal salts at elevated temperatures, and electroless deposition (ELD) from salt solutions using reducing agents or catalyst [15,20,21].

ELD is of particular interest because its simplicity can facilitate the large-scale production of nanotube-nanoparticle hybrids [4,7,22]. The ELD technique is particularly appealing because of its low cost, inherent selectivity and ability to deposit high quality films on very thin seed layers [23]. Thus far experimental studies have focused mainly on final or fully-metal deposited MWCNTs and their specialized applications. However, morphology of nanoparticles with process time or other factors (e.g. kinetics of the deposition process) has not been examined. The detailed structure and location of metal nanoparticles along a nanotube play an important role in determining the final assembled structure and its performance [24]. Therefore, studies on the morphology of metallic nanoparticles as a function of deposition time during the ELD process are needed in order to gain better understanding of the metal deposition of MWCNTs.

In this paper, silver (or copper) deposited MWCNTs were prepared using successively, surface oxidation (nitric acid-treatment), Sn–Pd

* Corresponding author. School of Mechanical Engineering, Yonsei University, Seoul 120-749, Republic of Korea. Tel.: +82 2 2123 2821; fax: +82 2 312 2821.
E-mail address: hwangjh@yonsei.ac.kr (J. Hwang).

0257-8972/$ – see front matter © 2008 Elsevier B.V. All rights reserved.
doi:10.1016/j.surfcoat.2008.09.017

activation, hydrochloric acid-acceleration, and ELD of silver (or copper). High resolution transmission electron microscopy (HRTEM), energy dispersive X-ray spectroscopy (EDX) and X-ray diffraction (XRD) were used to characterize the morphology and structure of the coated MWCNTs. The textural properties of the MWCNTs during the ELD process were examined using the Brunauer, Emmett, and Teller (BET) method [25].

2. Experimental

MWCNTs synthesized by a Korean company (Nanokarbon Co., Ltd.) were used for experiments. The mean inner diameter and length of the MWCNTs were ~50 nm and 20 μm, respectively. Fig. 1a shows the experimental procedure for silver (or copper) ELD onto the MWCNTs. Due to the strongly hydrophobic nature of MWCNTs, it was essential to activate their surfaces prior to the ELD process for bonding metal particles to them [26]. The cleaning and surface modification of the MWCNTs were carried out using a nitric acid (16 M) solution to produce adequate interface strength between the nanotubes and metals. The acid treatment was reported to produce –COOH, –OH, –C=O and other oxygen-containing functional groups [27] on the surfaces of the MWCNTs [18,27–31]. Then the Sn–Pd activation of the acid-treated MWCNTs was carried out as proposed by Ang et al. [10,11] to catalyze the surfaces of the MWCNTs and initiate the subsequent ELD of silver (or copper). The MWCNTs were stirred in a solution containing a mixture of 60 mL Sn–Pd colloid (28 mL of 0.5 M $SnCl_2$, 28 mL of 0.025 M $PdCl_2$, and 4 mL of 1 M HCl). In the Sn–Pd activation, the catalysts were believed to be Sn–Pd alloy [11] nuclei surrounded by a stabilizing layer of adsorbed Sn(+2) species (Tin chloride, oxide and hydroxide). The acceleration step (using 1 M of HCl) was used to remove the stabilizing layer of Sn(+2) species, which surrounds the Sn–Pd colloid particles and makes free their surface. After the washing step with 100 mL deionized (DI) water, the metallic Pd of the particles so-naked was then used to catalyze the ELD process, the silver (copper) ELD solution being in a metastable state. The metallic Pd on the surfaces of the MWCNTs would reduce silver (copper) ions

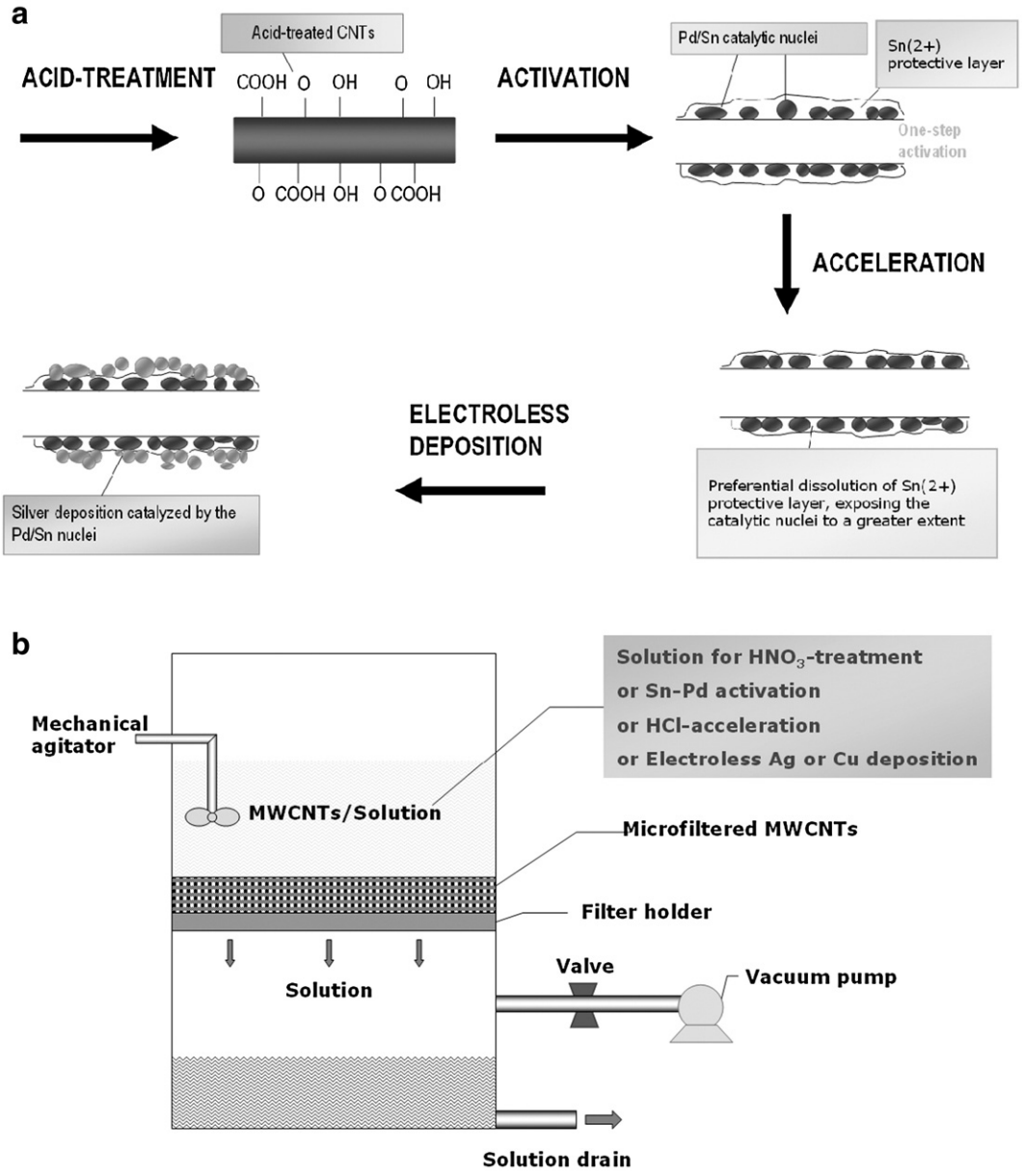

Fig. 1. (a) Processes for metallization. (b) Schematic of the microfiltration unit.

to silver (copper) atoms, where silver (copper) was further formed homogeneously (autocatalytic process). All processes including the HNO_3-treatment, Sn–Pd activation, and HCl acceleration, and ELD were performed in a 200 mL microfiltration unit, as shown in Fig. 1b. Each process time was determined by controlling the suction rate of the vacuum pump. The process times for the HNO_3-treatment, Sn–Pd activation, and HCl-acceleration steps were 5, 6, and 3 min, respectively.

After carrying out the pre-treatment processes, the MWCNTs were immersed into a solution for the ELD of silver (or copper). The silver ELD solution was a mixture of solutions A and B at a 1:1 (v/v) ratio [32]. Solution A contained 2 g of $AgNO_3$, 60 g of disodium ethylenediamine-tetraacetate (Na_2-EDTA), 88 mL of isopropyl alcohol, 12 mL of acetic acid and 400 mL of $NH_3{\cdot}H_2O$ in 1 L of DI water. Solution B contained 3 mL of hydrazine, 2 mL of mercerine and 400 mL of ethyl alcohol in 1 L of DI water. The copper ELD solution was a mixture of solutions C and D at a 10:1 (v/v) ratio [33]. Solution C contained 3 g of $CuSO_4$, 14 g of sodium potassium tartrate (Rochelle salt), and 4 g of NaOH in 100 mL of DI water. Solution D was an aqueous formaldehyde solution (37.2 wt.%). The pre-treated MWCNTs were immersed into the mixture of solutions A and B (or solutions C and D) for 3–10 min to allow silver (or copper) particles to deposit on the MWCNTs. A microfiltration was performed through a polytetrafluoroethylene (PTFE) membrane (Milipore, 0.22 μm pore size). Mechanical agitation during each process enhanced the dispersion of MWCNTs in each solution. All the above processes were operated at 20 °C. Finally, the silver (or copper) coated MWCNTs were washed three times in DI water and dried at 70 °C for 24 h.

A drop of a solvent containing the MWCNTs was placed onto carbon coated copper grids. The morphology of the MWCNTs was analyzed by transmission electron microscopy (TEM, JEM-2010) operated at 200 kV, HRTEM (JEM-3010) operated at 300 kV, and EDX (Oxford) operated at 15 kV. The size distributions of the metallic silver (or copper) were obtained by measuring the diameter D_i of each particle from four micrographs on different parts of the grid (magnification of 160,000). Depending on the experimental condition, the number of particles measured, n, ranged from 50 to 400. The standard deviation, σ, was calculated from the following equation:

$$\sigma = \left\{ \left[\sum (D_i - D)^2 \right] / [n-1] \right\}^{1/2} \quad (1)$$

where D is the average diameter.

XRD of the coated MWCNT was carried out using a Rigaku RINT-2100 diffractometer equipped with a nickel thin film attachment using Cu-Kα radiation (40 kV, 40 mA) having 0.15418 nm wavelength. The 2θ angles ranged from 10 to 90° with a speed of 4°/min by step scanning at an interval of 0.08°. The average crystallite size of the metallic silver (or copper) was calculated from the (111) diffraction peak. It is known that the decrease in width of a XRD peak shows the increase in size of the investigated crystal. The average crystallite size (t) is given as follows by the Scherrer formula [34],

$$t = 0.9\lambda / (\mathrm{FWHM}) \cos\theta \quad (2)$$

where λ is the wavelength of the X-rays, FWHM is the full width at half maximum reflection height (radians), and θ is the diffraction angle. The nitrogen adsorption isotherms of the MWCNTs were measured using a porosimeter (ASAP 2010, Micromeritics Ins. Corp., US) at 77.4 K at a relative pressure ranging from 10^{-6} to 1. High purity (99.9999%) nitrogen was used. All the samples were out-gassed at 573 K for two hours before each measurement. The specific surface area was determined using the BET equation [25]. The total pore volume was estimated based on the N_2 volume adsorbed at a relative saturation pressure (~0.996). The pore size distribution was determined using the Barrett, Joyner, and Halenda (BJH) method [35], which uses the area of the pore walls, and it employs the Kelvin equation to determine the correlation between the relative N_2 pressure in equilibrium and a porous solid with a pore size suitable for capillary condensation to occur.

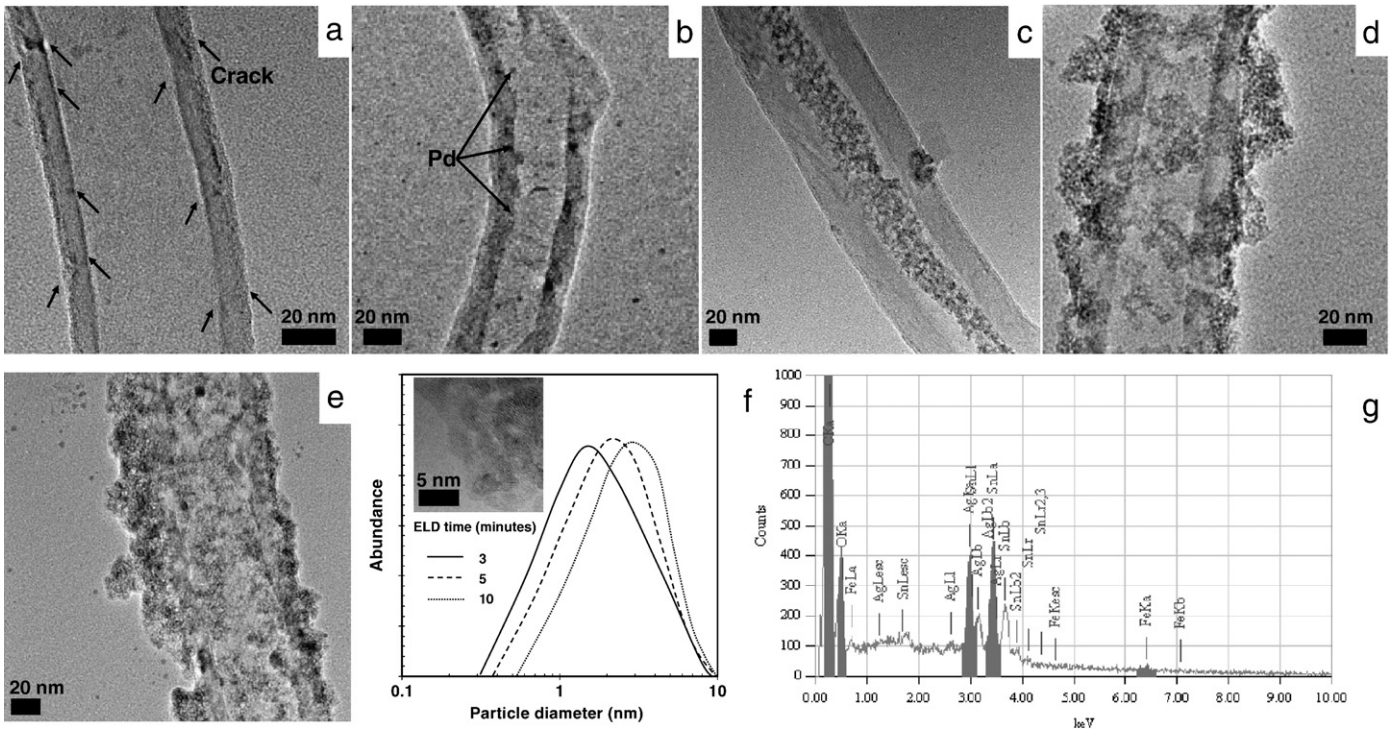

Fig. 2. Morphological and chemical analyses of MWCNTs. (a) HRTEM image of nitric acid-treated MWCNTs. (b) HRTEM image of Sn–Pd activated and accelerated MWCNTs. (c) HRTEM image of silver coated MWCNTs (for 3 min). (d) HRTEM image of silver coated MWCNTs (for 5 min). (e) HRTEM image of silver coated MWCNTs (for 10 min). (f) Particle size distribution of silver particles on MWCNTs from the HRTEM image. (g) EDX spectrum of silver deposited MWCNTs (for 5 min).

3. Results and discussion

3.1. Silver ELD on MWCNTs

Fig. 2a shows a HRTEM image of the acid-treated MWCNTs. Cracks in the image were generated on the MWCNTs due to acid attack (see arrows). Fig. 2b shows a HRTEM image of the MWCNTs after they were subjected to the activation and acceleration steps. Palladium particles (seen as tiny black spots in Fig. 2b) were not densely distributed over the tube-surfaces but were localized at various points along the tube, as discussed by Ang et al. [10]. These catalytic Pd particles were mainly 0.8 nm in diameter while particles larger than 0.8 nm were detected occasionally. Fig. 2c shows a HRTEM image of the MWCNTs after silver ELD for 3 min. At this stage, metallic silver, which appears as regions of darker contrast in the image, was deposited selectively on the interior surfaces of the MWCNTs due to the presence of concentrated chemical species, such as functional groups, Sn–Pd catalysts, silver ions and reductants on the interior surfaces. Capillary suction [36–38] might help the chemical species concentrated onto the interior surfaces of the MWCNTs. At the acid-treatment step, the interior surfaces of the MWCNTs might be effectively attacked by the acid allowing the formation of functional groups on the interior surfaces. In the subsequent Sn–Pd activation step, colloidal Sn–Pd species were also induced on the interior surfaces by capillary suction and then attached to the functional groups by adsorption [39]. When the ELD time was 5 min, metallic silver was deposited in both the interior and exterior surfaces of the MWCNTs, as shown in Fig. 2d. When the ELD time was extended to 10 min (Fig. 2e), the silver deposition layer grew laterally and vertically, completely covering the MWCNTs. For ELD of 5 and 10 min, the mean outer diameters of the coated MWCNTs were ~85 and ~105 nm, respectively. A closer examination of morphology of metallic silver on the exterior surface of the MWCNT (inset of Fig. 2f) revealed them to be agglomerates. According to image analyses, Fig. 2f shows that the average diameters of the metallic silver after ELD for 3, 5, and 10 min were 1.3±0.21, 1.9±0.33, and 2.6±0.34 nm, respectively. Fig. 2g shows the EDX spectrum for the silver deposited MWCNTs corresponding to Fig. 2d. The profile shows peaks for silver along with peaks for carbon and iron. The iron originated from commercial MWCNTs because iron had been used as the catalyst to synthesize the MWCNTs. The observed oxygen peak might have originated from the pre-treatment of the MWCNTs before silver ELD. Tin peaks were also detected; they are due to the Sn–Pd activation process. Although palladium was not detected by EDX, inductively coupled plasma atomic emission spectroscopy (ICP-AES) analyses indicated a palladium concentration of approximately 640 ppm, which was below the EDX detection limit. The silver-to-carbon fraction increased from 7.00 to 28.20% in mass (1.37 to 5.98% in atom) when the ELD time was increased from 3 to 10 min. Each mass ratio was measured using EDX with a mapping mode for lower magnitude image (×1000) than those in Fig. 2. The mass ratios were calibrated by blank data from pristine TEM grid as a reference. An exact value of the mass ratios was checked by inductively coupled plasma-atomic emission spectroscopy (ICP-AES, Elan 6000, Perkin-Elmer, US) and compared to EDX quantified results. The EDX results had ±7.4% error.

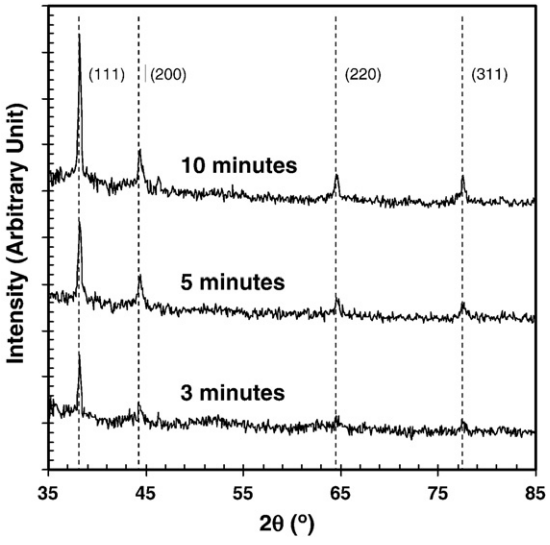

Fig. 3. XRD patterns of silver coated MWCNTs.

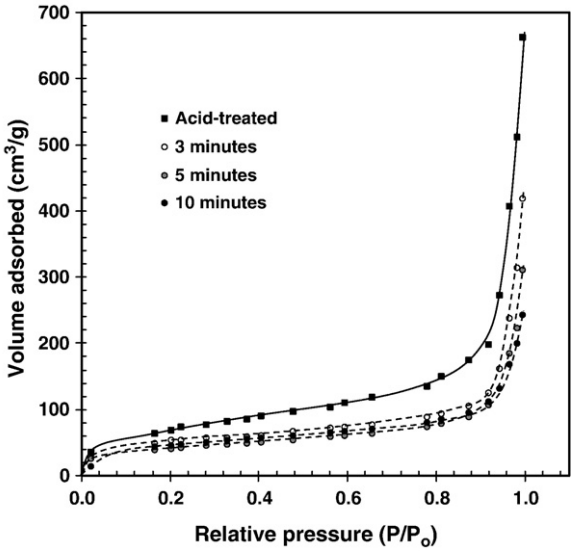

Fig. 4. Adsorption isotherms of silver coated MWCNTs.

Fig. 3 shows the XRD patterns highlighting the major diffraction peaks of the metallic silver. All XRD peaks were indexed to the silver face-centered-cubic (fcc) phase based on the joint committee on powder diffraction standards (JCPDS) data. The peaks at 38.2, 44.3, 64.5, and 77.4° 2θ were assigned to the (111), (200), (220), and (311) planes of the fcc phase of silver. The peak intensities increased with increasing ELD time, which suggests that the metallic silver area increased with increasing ELD time. The average crystallite sizes of the metallic silver calculated using the Scherrer formula were 0.9±0.09, 1.1±0.20, and 1.8±0.19 nm for an ELD time of 3, 5, and 10 min, respectively. The calculated sizes were smaller than those obtained from the HRTEM observations (1.3±0.21, 1.9±0.33, and 2.6±0.34 nm for 3, 5, and 10 min of ELD, respectively). However, these approximate values are comparable to the mean silver sizes calculated by HRTEM image analyses. As the Scherrer formula always tends to underestimate the real crystallite size [40], these results seem to favor the hypothesis of the monocrystallinity of the metallic silver.

Table 1
Textural properties of silver coated MWCNTs

Items samples	Total		Microporous		Mesoporous		APD[c] (Å)
	SA[a] (m^2/g)	PV[b] (cm^3/g)	SA (m^2/g)	PV (cm^3/g)	SA (m^2/g)	PV (cm^3/g)	
Acid-treated	261±23	1.02±0.08	61	0.16	200	0.86	194±8
3 min	194±16	0.68±0.05	44	0.12	150	0.56	172±8
5 min	163±18	0.48±0.06	37	0.08	126	0.40	155±4
10 min	144±18	0.38±0.06	31	0.03	112	0.35	110±6

[a] Surface area.
[b] Pore volume.
[c] Average pore diameter.

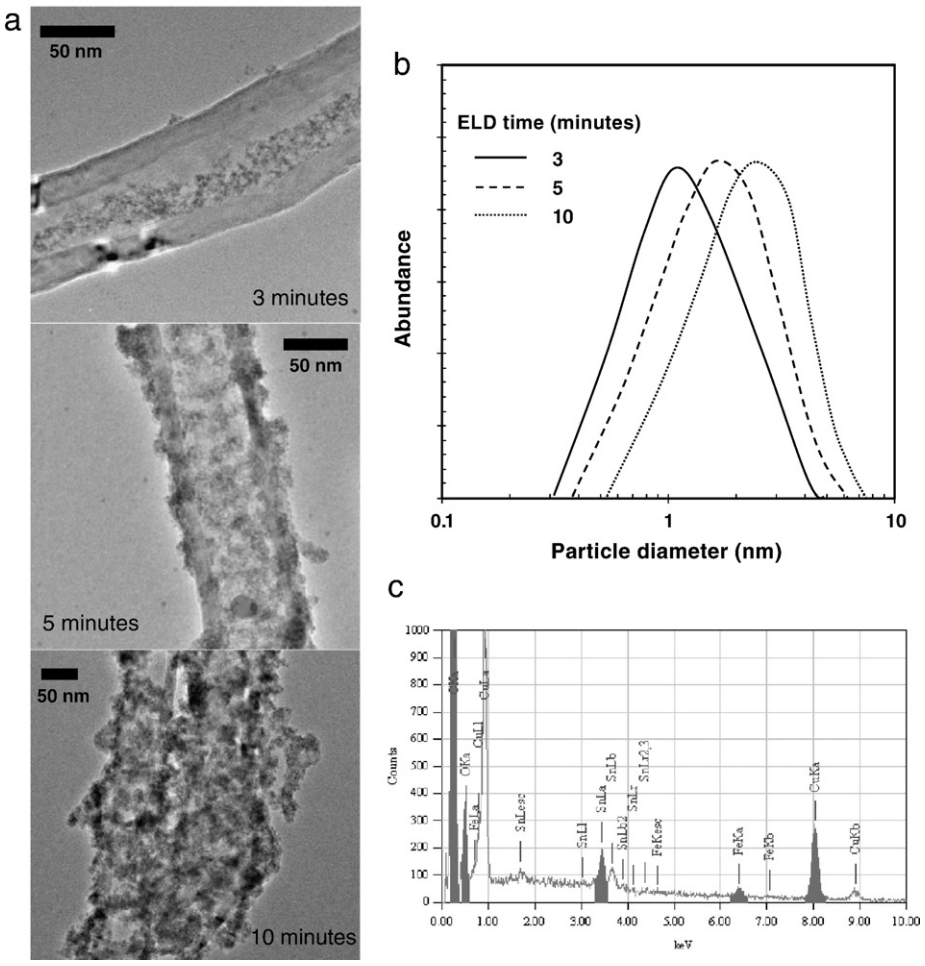

Fig. 5. Morphological and chemical characterizations of copper coated MWCNTs. (a) HRTEM micrographs. (b) Particle size distribution. (c) EDX spectrum.

Fig. 4 shows the nitrogen adsorption isotherms of MWCNTs at 77.4 K. The sharp increase in each curve from $P/P_o=0$ to 0.05 was attributed to rapid adsorption in the micropores of the MWCNTs. The curve increased slowly from $P/P_o=0.05$ to 0.85 due to capillary suction at the site of the mesopores [41]. Fig. 4 also shows a sharp increase in P/P_o ranging from 0.9 to 0.99 due to strong capillary condensation. All samples exhibited a type II adsorption isotherm according to the international union of pure and applied chemistry (IUPAC) classification, as reported by Rodriguez and Mackie et al. [42,43].

The amount of nitrogen adsorbed was inversely proportional to the ELD time. This was due to the blockage of pores in the MWCNTs by

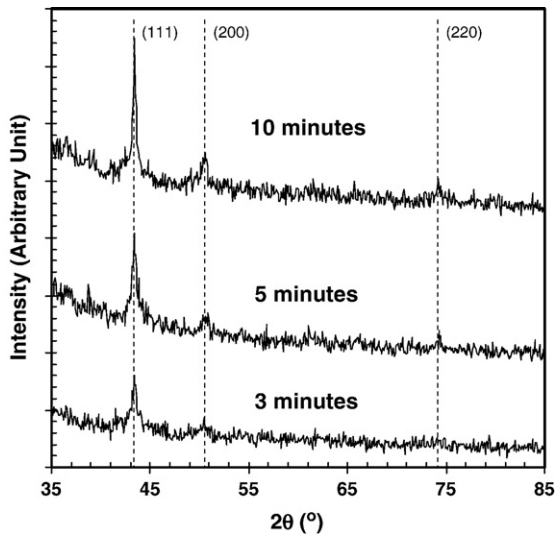

Fig. 6. XRD patterns of copper coated MWCNTs.

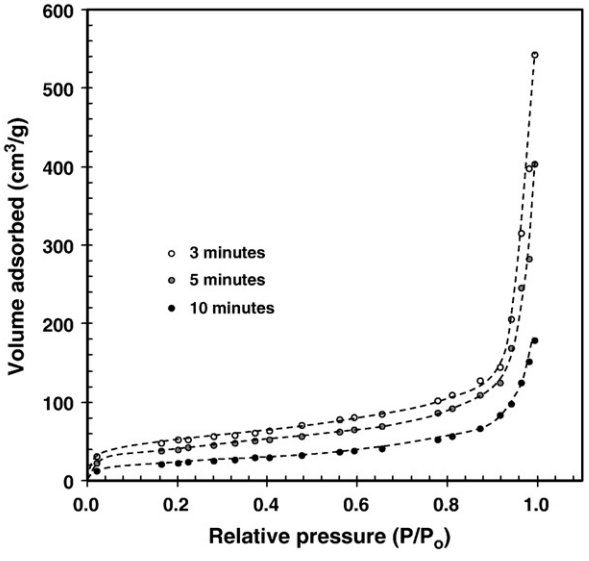

Fig. 7. Adsorption isotherms of copper coated MWCNTs.

Table 2
Textural properties of copper coated MWCNTs

Items samples	Total		Microporous		Mesoporous		APD[c] (Å)
	SA[a] (m^2/g)	PV[b] (cm^3/g)	SA (m^2/g)	PV (cm^3/g)	SA (m^2/g)	PV (cm^3/g)	
3 min	203±25	0.77±0.04	33	0.07	170	0.70	177±11
5 min	147±21	0.62±0.05	24	0.03	123	0.60	172±6
10 min	81±8	0.27±0.02	9	0.02	72	0.25	138±6

[a] Surface area.
[b] Pore volume.
[c] Average pore diameter.

silver particles, as shown by detailed results of BET analysis. Table 1 shows changes of surface areas and volumes of the micro and mesopores, and average pore diameter, with increasing ELD time. The ELD of 3 min caused a large decrease in porosity with most of the adsorptive sites being occupied within 3 min. However, the inherent mesoporous feature of MWCNTs (volume of mesopores>volume of micropores and average pore diameter>20 Å) [25] was retained, regardless of ELD time.

3.2. Copper ELD on MWCNTs

Fig. 5a shows HRTEM images of copper deposited MWCNTs when the ELD time increased from 3 to 10 min. The metallic copper were deposited selectively onto the interior surfaces of the MWCNTs. When the ELD time was 5 min, metallic copper was deposited on both the interior and exterior surfaces of the MWCNTs. The copper deposition layer further grew when the ELD time was prolonged to 10 min. Fig. 5b shows metallic copper size distribution and EDX spectrum. The mean diameters of the metallic copper were 1.1±0.14, 1.7±0.18, and 2.3±0.31 nm for 3, 5, and 10 min of ELD time, respectively. The EDX spectrum (Fig. 5c) showed peaks for copper, along with peaks for carbon, oxygen, iron, and tin. The copper-to-carbon fraction was increased from 6.66 to 25.51% in mass (0.90 to 4.60% in atom) when the ELD time was increased from 3 to 10 min. Although there were some minor differences in the metal-to-carbon fraction and average crystallite size between silver and copper ELD, the deposition morphology of metallic nanoparticles on the MWCNTs was similar for both silver and copper.

Fig. 6 gives the XRD profiles showing the major diffraction peaks for metallic copper. The peaks at 43.2, 50.3, and 74.1° 2θ were assigned to the (111), (200), and (220) planes of the fcc phase of copper. The average crystallite sizes of the metallic copper calculated using the Scherrer formula were 0.7±0.10, 1.9±0.22, and 1.4±0.18 nm for an ELD time of 3, 5, and 10 min, respectively.

Fig. 7 shows the nitrogen adsorption isotherms of the copper deposited MWCNTs at 77.4 K. All sampled exhibited a type II isotherm according to the IUPAC classification [42,43]. The BET data of Table 2 show that the inherent mesoporous feature of MWCNTs (volume of mesopores>volume of micropores and average pore diameter>20 Å) [25] was also retained, as in the case of silver deposition, regardless of ELD time.

3.3. Silver ELD on thin-MWCNTs

The TEM images (Fig. 8a–c) show that metallic silver (10–80 nm) much larger than those in the Sections 3.1 and 3.2 (~1.5 nm) were deposited only on the exterior surfaces of the thin-MWCNTs (~5 nm in inner diameter and 10–20 μm in length; CMP-340F, Iljin Nanotech, Korea) because the capillarity decreases with decreasing tube diameter, as reported by Ugarte et al. [36], who suggested that the capillarity depends on the inner diameter of the MWCNTs and that the nanotube-liquid interface energy decreases with decreasing inner diameter. The capillarity inside the tubular cavities and/or interstitial spaces between CNTs is described as follows [44,45];

$$E_{\text{capilarity}} = -2rl\cos\theta_E \tag{3}$$

where $E_{\text{capilarity}}$ is the energy gain for the capillary filling of a CNT, r is the radius of inner cavity, and l is the length of cavity.

Even though the inner diameters of the thin-MWCNTs were as large as those used by Ugarte et al. [36,37] (~4 nm) for silver filling, the difference between their results and ours might be due to the different reaction conditions (e-beam decomposition of silver nitrate vs ELD of silver) and/or mass transfer inhibition by the formerly deposited silver particles near the open end of the thin-MWCNTs, as shown in Fig. 8d. The formation of metallic silver much larger than those in the Section 3.1 cases might be due to the high number of catalytically activated sites. For thin-MWCNTs, unlike the Section 3.1 cases, the activated sites would exist only on the exterior surfaces, so rapid nucleation and

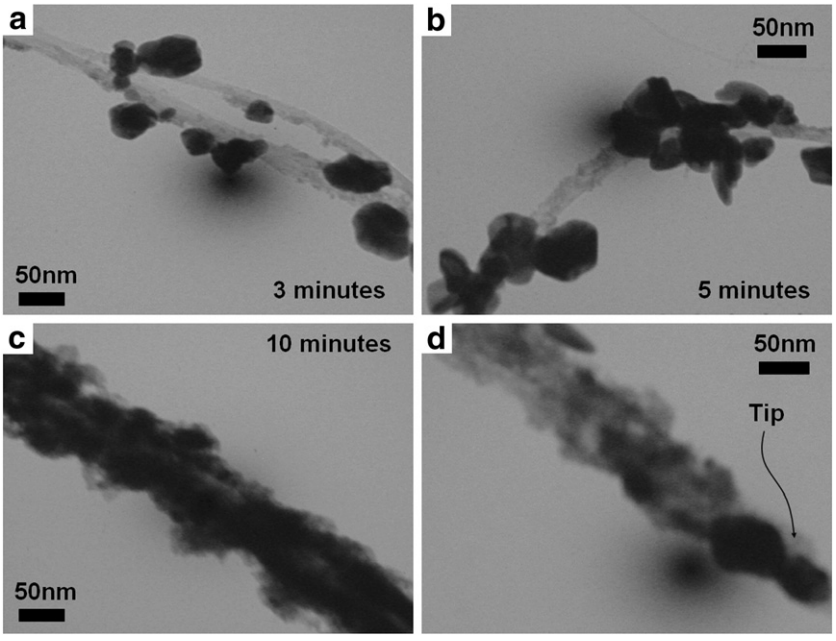

Fig. 8. TEM micrographs of silver deposited thin-MWCNTs for (a) 3, (b) 5, and (c) 10 min. (d) TEM image near open end of thin-MWCNTs (for 5 min of ELD).

the subsequent deposition of silver on the exterior surfaces could be achieved.

4. Concluding remarks

In this study, the effects of ELD time and diameter of a multi-walled carbon nanotube on deposition characteristics of silver (or copper) nanoparticles were investigated. Although there were some minor differences, such as the metal-to-carbon fraction and average crystallite size between silver and copper ELD, the deposition results were similar for both silver and copper. When the ELD time was 3 min, nanoparticles of fcc silver (or copper) were deposited on the interior surface of a MWCNT (~50 nm in inner diameter). When the ELD time was 5 min, fcc silver (or copper) was deposited in both the interior and exterior surfaces of the MWCNT. When the ELD time was extended to 10 min, fcc silver (or copper) deposition layer grew laterally and vertically, completely covering the MWCNT. However, there was no silver deposition on the interior surface of a thin-MWCNT (~5 nm in inner diameter) observed because the capillarity decreases with decreasing tube diameter.

In this study, metal-encapsulated (inner coating) MWCNTs, metal-surrounded (outer coating) MWCNTs, and both metal-encapsulated and surrounded MWCNTs were obtained, depending on ELD time and tube diameter. Therefore, all depositions times led to structures with features (nature of porosity, coverage, morphology, etc.) that are promising for reservoirs in catalysis, fuel cells, sensors, data storage, template synthesis, and etc., depending on type of metal and view of unique structure of metal deposited MWCNTs.

Acknowledgement

This study was supported by Seoul R&DB Program (Grant No. 10593).

References

[1] V. Georgakilas, D. Gournis, V. Tzitzios, L. Pasquato, D.M. Guldi, M. Prato, J. Mater. Chem. 17 (2007) 2679.
[2] S. Iijima, J. Chem. Phys. 104 (1996) 2089.
[3] R. Saito, M. Fujita, G. Dresselhaus, M.S. Dresselhaus, Appl. Phys. Lett. 60 (1992) 2204.
[4] P. Calvert, Nature 357 (1992) 365.
[5] G.G. Wildgoose, C.E. Banks, R.G. Compton, Small 2 (2006) 182.
[6] G. Che, B.B. Lakshmi, C.R. Martin, E.R. Fisher, Langmuir 15 (1999) 750.
[7] L. Qu, L. Dai, J. Am. Chem. Soc. 127 (2005) 10806.
[8] J.M. Planeix, N. Coustel, B. Coq, V. Brotons, P.S. Kumbhar, R. Dutartre, P. Geneste, P. Bernier, P.M. Ajayan, J. Am. Chem. Soc. 116 (1994) 7935.
[9] D. Yuan, Y. Liu, Rare Metals 25 (2006) 237.
[10] L.M. Ang, T.S.A. Hor, G.Q. Xu, C.H. Tung, S.P. Zhao, J.L.S. Wang, Chem. Mater. 11 (1999) 2115.
[11] F.Z. Kong, X.B. Zhang, W.Q. Xiong, F. Liu, W.Z. Huang, Y.L. Sun, J.P. Tu, W.X. Chen, Surf. Coat. Technol. 155 (2002) 33.
[12] Z. Liu, X. Lin, J.Y. Lee, W. Zhang, M. Han, L.M. Gan, Langmuir 18 (2002) 4054.
[13] G. Vijayaraghavan, K.J. Stevenson, Langmuir 23 (2007) 5279.
[14] L. Jiang, L. Gao, Carbon 41 (2003) 2923.
[15] H.C. Choi, M. Shim, S. Bangsaruntip, H. Dai, J. Am. Chem. Soc. 124 (2002) 9058.
[16] Q. Xu, L. Zhang, J. Zhu, J. Phys. Chem. B 107 (2003) 8294.
[17] S. Fullam, D. Cottell, H. Rensmo, D. Fitzmaurice, Adv. Mater. 12 (2000) 1430.
[18] B.K. Pradhan, T. Toba, T. Kyotani, A. Tomita, Chem. Mater. 10 (1998) 2510.
[19] T.M. Day, P.R. Unwin, N.R. Wilson, J.V. Macpherson, J. Am. Chem. Soc. 127 (2005) 10639.
[20] M. Hasegawa, N. Yamachika, Y. Shacham-Diamond, Y. Okinaka, R. Osaka, Appl. Phys. Lett. 90 (2007) 101916.
[21] B. Kim, W.M. Sigmund, Langmuir 20 (2004) 8239.
[22] T.W. Ebbesen, H. Hiura, M.E. Bisher, M.M.J. Treacy, J.L. Shreeve-Keyer, R.C. Haushalter, Adv. Mater. 8 (1996) 155.
[23] W.X. Chen, J.P. Tu, H.Y. Gan, Z.D. Xu, Q.G. Wang, J.Y. Lee, Z.L. Liu, X.B. Zhang, Surf. Coat. Technol. 160 (2002) 68.
[24] L. Qu, L. Dai, E. Osawa, J. Am. Chem. Soc. 128 (2006) 5523.
[25] S. Brunauer, P.H. Emmett, E. Teller, J. Am. Chem. Soc. 60 (1938) 309.
[26] Q. Li, S. Fan, W. Han, C. Sun, W. Liang, Jpn. J. Appl. Phys. 36 (1997) L501.
[27] C.-S. Chen, X.-H. Chen, Z. Yang, W.-H. Li, L.-S. Xu, B. Yi, Diamond Relat. Mater. 15 (2006) 151.
[28] R. Yu, L. Chen, Q. Liu, J. Lin, K.-L. Tan, S.C. Ng, H.S.O. Chan, G.-Q. Xu, T.S.A. Hor, Chem. Mater. 10 (1998) 718.
[29] Y. Feng, H. Yuan, J. Mater. Sci. 39 (2004) 3241.
[30] Y. Xing, J. Phys. Chem. B 108 (2004) 19255.
[31] C. Xu, J. Chen, Y. Cui, Q. Han, H. Choo, P.K. Liaw, D. Wu, Adv. Eng. Mater. 8 (2006) 73.
[32] J.H. Byeon, J.H. Park, K.Y. Yoon, J. Hwang, Langmuir 24 (2008) 5949.
[33] J.H. Byeon, K.Y. Yoon, Y.K. Jung, J. Hwang, Electrochem. Commun. 10 (2008) 1272.
[34] K. Ada, M. Gökgöz, M. Önal, Y. Sarikaya, Pow. Technol. 181 (2008) 285.
[35] E.P. Barrett, L.G. Joyner, P.P. Halenda, J. Am. Chem. Soc. 73 (1951) 373.
[36] D. Ugarte, W. Châtelain, W.A. de Heer, Science 274 (1996) 1897.
[37] D. Ugarte, T. Stöckli, J.M. Bonard, W. Châtelain, W.A. de Heer, Appl. Phys. A 67 (1998) 101.
[38] P.M. Ajayan, S. Iijima, Nature 361 (1993) 333.
[39] B.C. Satishkumar, E.M. Vogl, A. Govindaraj, C.N.R. Rao, J. Phys. D 29 (1996) 3173.
[40] P.-Y. Silvert, R. Herrera-Urbina, K. Tekaia-Elhsissen, J. Mater. Chem. 7 (1997) 293.
[41] M. Chen, H.-W. Yu, J.-H. Chen, H.-S. Koo, Diamond Relat. Mater. 16 (2007) 1110.
[42] N.M. Rodriguez, J. Mater. Res. 8 (1993) 3233.
[43] E.B. Mackie, R.A. Wolfson, L.M. Arnold, K. Lafdi, A.D. Migone, Langmuir 13 (1997) 7197.
[44] Q. Fu, W. Gisela, D.-S. Su, New Carbon Mater. 23 (2008) 17.
[45] G.L. Aranovich, M.D. Donohue, J. Colloid Interf. Sci. 292 (2005) 202.